Nanoscale

Enhancing EMI shielding of natural rubber-based supercritical CO2 foams by exploiting porous morphology and CNT segregated network

Journal:	*Nanoscale*
Manuscript ID	NR-ART-09-2018-007351.R1
Article Type:	Paper
Date Submitted by the Author:	26-Nov-2018
Complete List of Authors:	Zhan, Yanhu; CNR-Institute of Composite and Biomedical Materials; Liaocheng University, Department of Materials Science and Engineering Oliviero, Maria; CNR IPCB Wang, Jian; State Key Laboratory of Polymer Materials Engineering, Polymer Research Institute, Sichuan University Sorrentino, Andrea; CNR-Institute of Composite and Biomedical Materials Buonocore, Giovanna; CNR-Institute of Composite and Biomedical Materials, Sorrentino, L.; CNR Lavorgna, Marino; CNR-Institute of Composite and Biomedical Materials, Xia, Hesheng; Polymer Research Institute, Sichuan University, Iannace, Salvatore; d. Institute for Macromolecular Studies (ISMAC-CNR) National Research Council

Nanoscale

ARTICLE

Enhancing EMI shielding of natural rubber-based supercritical CO_2 foams by exploiting porous morphology and CNT segregated network †

Received 00th January 20xx,
Accepted 00th January 20xx

DOI: 10.1039/x0xx00000x

www.rsc.org/

Yanhu Zhan, [a,b,#] Maria Oliviero, [a,#] Jian Wang, [c] Andrea Sorrentino, [a] Giovanna G. Buonocore, [a] Luigi Sorrentino, [a] Marino Lavorgna, *[a] Hesheng Xia [c] and Salvatore Iannace [d]

Natural rubber/carbon nanotubes composite foams (F-NR/CNTs) with high electrical conductivity and excellent electromagnetic interference (EMI) performance were developed through a multi-steps process including: a) CNTs assembling on natural rubber latex particles, b) pre-crosslinking of natural rubber, c) supercritical carbon dioxide foaming of pre-crosslinked composite samples and d) post-crosslinking of foamed composite samples. Closed-cell porous structure and segregated-CNT network are clearly observed in the resulting foams. Due to this morphology, F-NR/CNTs exhibit low density, good mechanical properties, and high electrical conductivity. Owing to the multiple radiation reflections and scattering between the cell-matrix interfaces, the composite foams presented an excellent specific shielding effectiveness (SSE) of 312.69 dB cm^2/g for F-NR/CNTs containing 6.4wt% of CNTs, which is significantly higher than those already published for rubber composites containing comparable filler content. Furthermore, the analysis of EMI SE highlights that absorption efficiency is more significant than reflection efficiency, implying that most of incident electromagnetic radiation is dissipated in form of heat. This work provides the fundamentals for the design of innovative lightweight and efficient EMI shielding foams, characterized by a three-dimensional segregated CNTs network with valuable potentials in the electronics and aerospace industries.

Introduction

Due to the prevalence of digital devices and the rapid development of radar detecting technology, electromagnetic interference (EMI) has become a relevant societal concern since it affects the functionality of electronic devices and may have negative effects on people health.[1] In order to mitigate this technological and safety issues, high-performance EMI shielding polymer-based composites have recently attracted high attention of both academic institutions and industrial companies.[1-3] The EMI shielding effectiveness (EMI SE) of these composites is a measure of their ability to attenuate electromagnetic waves and it strongly depends on electrical conductivity and thickness of materials. The inclusion in polymers of high content of conductive filler, such as carbon black (CB), carbon nanotubes (CNTs) and graphene nanoplatelets and its derivatives (GE), brings about outstanding improvement of both electrical conductivity and EMI SE of the resulting composite materials. [4] Unfortunately, their density is often higher than that of pristine polymer thus limiting their application in specific fields such as aerospace, automobile industries, and portable electronics. In this context, the design and development of lightweight porous polymer composites exhibiting excellent EMI shielding properties represents an important challenge to be addressed for promising technological applications. [5,6]

In the wide panorama of the polymer-based nanocomposites, the tailoring of the spatial distribution of filler as a three-dimensional network, often referred to as segregated morphology, has been widely investigated by some of the authors and it has been proved to be an effective approach in improving electrical conductivity and, consequently, EMI SE of materials.[7-13] In details, the conductive fillers such as GE as well as carbon nanotubes are firstly assembled at the interfaces of polymer particles generally trough a solvent-wrapping or an ultrasonic assisted latex-based assembling approach. Then, by applying a coagulation/compression treatment, the conductive filler segregates in the excluded volume between the polymer particles. In this system a significant reduction of percolation threshold was achieved, [8-10] indeed the amount of filler needed to trigger the formation of a conductive network is much lower than that necessary when the filler is randomly dispersed within the polymer matrix. Jia and co-workers [11] performed a comparative study of EMI shielding performance of polyethylene (PE)/CNT composites with and without CNT-based segregated structure. They found that EMI SE of materials containing only 5wt% of filler with the segregated network was equal

[a] Institute of Polymers, Composites and Biomaterials, National Research Council, P.le Fermi, 1-80055 Portici, NA, Italy. E-mail address: mlavorgn@unina.it
[b] School of Materials Science and Engineering, Liaocheng University, Liaocheng 252000, China
[c] State Key Laboratory of Polymer Materials Engineering, Polymer Research Institute, Sichuan University, Chengdu 610065, China
[d] Institute for Macromolecular Studies (ISMAC-CNR) National Research Council, Milano 20133, Italy.
# These authors contributed equally to this work.
† Electronic Supplementary Information (ESI) available: The scheme of procedure for NR/CNTs foams; TEM images of $NR/CNT_{1.68}$ and $NR/CNT_{6.40}$ foams; EMI properties of N-NR/CNTs composites; Mechanical properties of N-NR/CNTs composites. See DOI: 10.1039/x0xx00000x

to 46.4 dB, which was about 46% higher than that shown by the composite with 5wt% of randomly distributed CNT. The same authors [12] also realized a segregated natural rubber/CNT composite which, again, showed a high EMI SE value (33.3 dB) even at low CNT content (5wt%). Moreover, in a previous paper of them, NR/GE and NR/Fe_3O_4@GE composites with segregated network, prepared by latex mixing method, exhibited EMI SE values equal to 34.0 dB and 42.4 dB at 9.0 GHz, respectively. [13]

A further significant improvement of the functional properties of conductive composites may be obtained by exploiting the concept of conductive lightweight materials.[14-16] In these materials, the micron-sized cells not only reduce the density of materials but may also increase significantly absorption of electromagnetic waves, resulting from the multiple reflection effects of the incident waves in the porous architectures.[15] Supercritical CO_2 ($ScCO_2$) foaming processes, a physical foaming method, is one of the most preferable approach to produce porous materials since it is somewhat inexpensive, and essentially nontoxic and environmentally friendly.[17] Many polymers, such as PE,[18] polyvinyl chloride,[19] polyetherimide,[20] polycarbonate (PC),[21] polystyrene,[22] PMMA,[23] polylactic acid (PLA),[24] poly(ethylene terephthalate), [25] and silicon rubber, [26] as well as blends (such as poly(butylene succinate)/thermoplastic gelatin[27]) can be foamed by $ScCO_2$ process. Zhang et al.[6] produced by $ScCO_2$ foaming process lightweight PMMA/Fe_3O_4@CNT foams characterized by density in the range 0.22-0.38 g/cm^3 and EMI SE equal to 13.1 dB. Gedler et al.[21] found that EMI SE of porous PC/GE foamed by $ScCO_2$ foaming process is approximately 10 times higher than that of compact composite containing the same GE amount. EMI shielding properties of the polymer foams are dependent on their electrical conductivity according to EMI shielding theory. During foaming, the conductive filler is redistributed and additional effective conductive paths form when expansion happen in a constrained mold. On the other side, when the foaming is performed in free expansion, the average distance between conductive filler particles increases, with a consequent reduction of effective conductive paths. Thus the electrical conductivity and EMI shielding properties depends of foaming process and on the expansion ratio. Meanwhile, the porous structure increases significantly the absorption of electromagnetic waves because of the improved multiple reflection effects of the incident waves. By contrast, the cell walls may become noticeable thin or cracked when the foaming degree is very high, so the effective conductive paths decrease, bringing about a sharp reduction of electrical conductivity and EMI shielding properties.[16] For polymer composites with segregated filler network, their electrical conductivity and EMI shielding properties decrease after foaming because of the formation of some discontinuous segregated network during foaming process, even at low foaming degree. However, it still is interesting to prepared filler/polymer composite foams with segregated network because of their low density. For example, Wang et al.[24] firstly prepared porous PLA beads foamed by $ScCO_2$ and then wrapped CNT upon the porous beads in order to construct a segregated CNT network after steam-chest molding process. This material exhibited an excellent EMI shielding performance (~46 dB) which was ascribed to the synergistic effect between fine microporous structure and the conductive CNT networks.

In this context, porous EMI shielding composite materials prepared by using natural rubber (NR) and exhibiting a segregated network of conductive filler are very promising for their capability to withstand extreme temperatures and environmental conditions alongside with their ability to absorb high impact energy and attenuate EMI waves.[28,29] So far, however, the foamed NR composites, with random dispersion of filler, are prepared mainly by chemical foaming process.[30,31] In fact, it is a big challenge to fabricate porous rubber with segregated network, even more by $ScCO_2$ foaming method. This difficulty is ascribed to the ultralow glass transition temperature of rubber, which results in a complex control of concomitant polymer reaction and foaming processes such as cell nucleation and growing and natural rubber crosslinking. Without a fine control of these concomitant processes, the cells formed after CO_2 expansion may collapse during crosslinking process. On the contrary, whether the foaming procedure is conducted after crosslinking process, the crosslinked rubber does not foam by $ScCO_2$ method.

Herein, the authors propose a new method to prepare porous composites of NR with CNTs segregated network, namely segregated F-NR/CNTs, by means of a fine control of the two concomitant processes, i.e. rubber crosslinking and $ScCO_2$ foaming. In brief, segregated composites, namely segregated N-NR/CNTs were prepared by first wrapping CNTs around the latex particles which were then densified and pre-crosslinked at 120 ^oC and finally foamed by $ScCO_2$ method. Subsequently, the F-NR/CNTs specimens were quickly crosslinked at 170 ^oC. The morphology, thermal, electrical, EMI shielding and mechanical properties of the foamed composites with segregated network were deeply investigated. All the results confirm that the excellent EMI shielding performance of the obtained samples is ascribed to the synergistic effect of the segregated network of carbon nanotubes and the micro-cellular structure of the foamed natural rubber composites.

Experimental Section

Materials

Natural rubber latex (LCS, solid content: 67.5wt%) was supplied by Synthomer (UK). Dicumyl peroxide (DCP) was provided from Acros Organics (Thermo Fisher Scientific, Belgium). Carbon nantube (NC 7000, diameter: 10 nm, length: 1.5 μm, density: 1.75 g/cm^3) were purchased from Nanocyl S.A., Belgium. Cetyltrimethylammonium bromide (CTAB), as a surfactant, was obtained from Sigma Aldrich Chemicals (USA). All agents are used without further purification.

Preparation of segregated F-NR/CNTs composite foams

The preparation of F-NR/CNTs with the segregated morphology was performed through a multistep process consisting of a) CNT assembling on natural rubber latex particle, b) pre-crosslinking of natural rubber obtained through filtration from latex dispersion, c) $ScCO_2$ foaming process of the pre-crosslinked sample and d) post-crosslinking of foamed samples. In details a certain amount of CNT and CTAB with a CNT/CTAB weight ratio of 1:4 were uniformly dispersed into water by using an ultrasound probe (UP200S Hielscher sonifier, temperature: 0°C, cycle: 0.5, amplitude: 80%) for 30 min. Natural rubber latex was added into the obtained solution containing

0.5 g/L CNT by ultrasound for 30 min. DCP was then added and stirred vigorously for further 10 min at 50 °C. Afterwards, the obtained dispersion was filtered, washed and dried. Several rubber composites were prepared, whose formulations are reported in Table 1. In order to produce pre-crosslinked rubber sheet specimens, the various formulations were compression molded at 120 °C and 10 bar for 3 min and then cooled at room temperature. With this procedure it was possible to preserve the segregated morphology originated by the tailored assembling of CNTs around the NR latex particles. The several composites with segregated network were denoted as N-NR/CNT_x, where *x* was the CNTs concentration expressed as weight percentage of CNTs with respect to the natural rubber.

N-NR/CNT_x sheet specimens were placed into high pressure vessel and saturated with $ScCO_2$ at 40 bar and 35 °C for three times: 30, 60 and 120 min. After saturation time, the high-pressure CO_2 was released quickly to atmospheric pressure and samples were foamed. Finally, the foamed specimens were quickly (in the range of a few seconds) placed into an oven at 170 °C for 90 s in order to further crosslink the natural rubber. The procedure is schematized in Fig. S1.

In addition, the composite with 3.31 wt% of CNTs was further mixed by Haake Mini-Lab twin-screw extruder (Thermo Electron Corp., Hamburg, Germany) at room temperature for 10 min. Then, this composite was pre-crosslinked, foamed and post-crosslinked following the same procedures previously described for samples with segregated network. The obtained NR/$CNT_{3.31}$ composite with not-segregated morphology was designated as R-NR/$CNT_{3.31}$.

Characterization

Structure analysis: Particles of NR latex with and without CNT were characterized by using an optical microscope (Olympus Cover-018, Japan). A Quanta 200 F (Fei Company, USA) SEM instrument was utilized to characterize the surface morphologies of the fractured composites. In details, the specimens were cryogenically fractured in liquid nitrogen and sputter coated with gold before observation. The resulting micrographs were analyzed by Nano Measurer software to determine the cell average diameter, distribution of cell size and cell density. In particular, the cell density (N_f) can be estimated according to Equation (1), [32] where *n* is the number of bubbles in the area observed in the micrograph, *M* is the magnification factor, and K is the expansion ratio:

$$N_f = (nM^2/A)^{3/2} \cdot K \quad (1)$$

Table 1. Compositions of N-NR/CNTs composites

Sample	NR latex (g)	CNT (g)	CTAB(g)	DCP(g)
NR	8.3	0	0	0.25
N-NR/$CNT_{0.82}$	8.3	0.05	0.2	0.25
N-NR/$CNT_{1.68}$	8.3	0.1	0.4	0.25
N-NR/$CNT_{3.31}$	8.3	0.2	0.8	0.25
N-NR/$CNT_{4.87}$	8.3	0.3	1.2	0.25
N-NR/$CNT_{6.40}$	8.3	0.4	1.6	0.25

The rubber latex and the CNTs segregated network present within the several composites were observed by means of a transmission electron microscope (TEM) (Tecnai Spirit; FEI Co., USA) operating at 120 kV. Images were recorded with a MegaView G2 CCD camera (Olympus, Japan). The composites were cryomicrotomed by using a Leica EM FC3 equipment to get the ultrathin sections of 70-80 nm thickness, which were collected and directly supported on a copper grid for observation.

Electrical conductivity measures: The conductivity of all composite samples were measured by a two-point measurement (2400 picoameter, Keithley, USA). Rectangular samples (10×5×1.3 mm^3) were cut and coated by using silver epoxy paste to improve the electrical contact between picoameter electrodes and the sample surface.

Thermal analysis: A TA Discovery DSC instrument was used to investigate the thermal properties of the composites in nitrogen atmosphere. The samples were firstly cooled to -80 °C with liquid nitrogen and then heated up to -35 °C at a rate of 10 °C/min. Thermal properties were investigated by using a TGA Q600 (TA Instruments, USA) operating in a nitrogen atmosphere. Samples were heated from 50 to 600 °C at a heating rate of 10 °C/min.

Mechanical properties: Compression property of the composite samples were measured by using a TA Q800 DMA instrument (TA Instruments, USA) under a ramp strain of 5%/min at the room temperature. The dimensions of the samples were 7×7×7 mm^3.

EMI performance: EMI SE of the composite samples with a thickness of 1.3 mm was evaluated by the vector network analyzer, N5247A from Agilent (USA), in transmission-reflection mode. The scattering parameters (S_{11} and S_{21}) in the frequency range between 8.2 and 12.4 GHz (X-Band) were recorded. From S_{11} and S_{21} scattering parameters, the power coefficients of reflectivity (*R*), transmissivity (*T*), and absorptivity (*A*) can be obtained by using the following Equation (2), (3) and (4): [33]

$$R = |S_{11}|^2 \quad (2)$$

$$T = |S_{21}|^2 \quad (3)$$

$$A = 1 - R - T \quad (4)$$

The total EMI SE (SE_{Total}), defined as the logarithmic ratio of incoming (P_{in}) to outgoing power (P_{out}) of electromagnetic radiation was also calculated, according to the Equation (5): [34]

$$SE_{Total} = -10lg(\frac{P_{out}}{P_{in}}) = SE_R + SE_A + SE_M \quad (5)$$

where SE_A, SE_R, and SE_M are the absorption shielding, reflection shielding, and multiple reflections shielding, respectively. The SE_M usually can be neglected when SE_{Total}>10 dB. Thus SE_{Total} can be simplified to Equation (6):

$$SE_{Total} = SE_R + SE_A \quad (6)$$

where SE_R and SE_A can be obtained from the following Equation (7) and (8): [33]

$$SE_R = -10lg(1-R) \quad (7)$$

$$SE_A = -10lg(\frac{T}{1-R}) \quad (8)$$

where *T* and *R* are reflectivity and transmissivity, respectively, as reported in Equation (2) and Equation (4).

Results and discussion

Morphology of NR latex particles with and without assembled CNTs

In order to get NR/CNTs composites with CNTs segregated network, NR latex particles were firstly mingled with CNTs aqueous dispersion containing CTAB under ultrasonic conditions by promoting CNT wrapping on latex particles. The morphology of NR latex particles with and without CNTs was observed by optical microscope (selected images are shown in Fig. 1). Contrary to the pristine NR latex (Fig. 1a)), in presence of CNTs and CTAB, the NR particles appear uniformly dispersed, as shown in Fig. 1b). This confirms the formation of a stable NR/CNTs system, which is beneficial for the attainment of the segregated CNT network. The effectiveness of the CNTs assembling process is evaluated by the TEM analysis (Fig. 1c) and d)). After the CNTs assembling process, rubber particles are uniformly coated with CNTs which are well attached to the rubber particles at one end whereas the other ends often float in the solvent. Furthermore, from Fig.s 1d and S2, it is clearly observed that the sonication does not fragment the CNTs during preparation of NR/CNT latex dispersion. Thus, the CNTs with original 1.5 µm length can significantly contribute to improve electrical conductivity and EMI shielding properties of NR/CNT composites.

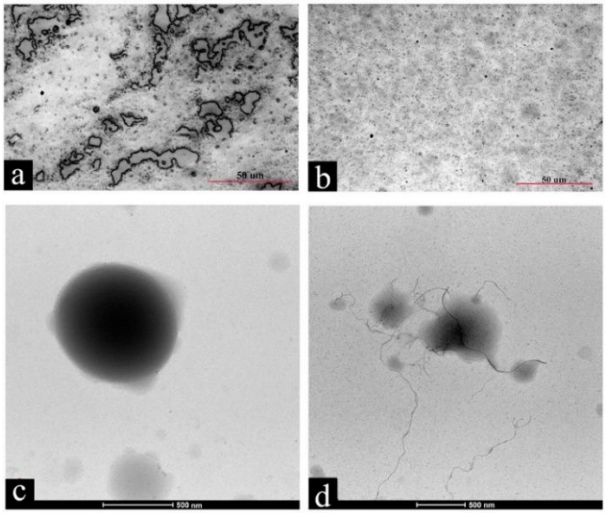

Fig. 1. Optical microscopy images of a) NR latex and b) NR latex containing 3.31wt% CNTs. TEM images of c) NR latex particle and d) NR latex particles coated with 3.31wt% CNTs

Table 2. Mean cell diameter and cell density of F-NR/CNTs composite foams

Sample	Saturation time (min)	Mean cell diameter (µm)	Cell density (cells/cm^3)
NR foam	60	13.46	2.11×10^8
F-NR/CNT$_{1.68}$	60	23.11	1.04×10^8
F-NR/CNT$_{3.31}$	30	5.51	4.85×10^8
F-NR/CNT$_{3.31}$	60	8.57	3.58×10^8
F-NR/CNT$_{3.31}$	120	6.32	5.45×10^8
F-NR/CNT$_{4.87}$	60	3.92	1.77×10^9

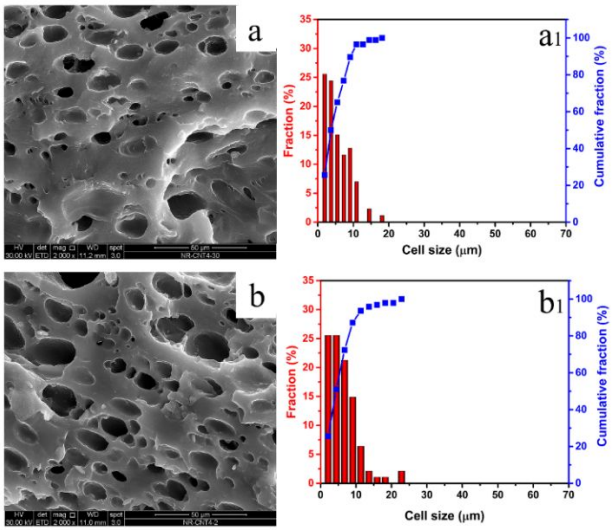

Fig. 2. Cell morphology and size distribution of F-NR/CNT$_{3.31}$ composite foams obtained at $ScCO_2$ saturation time: a) and a$_1$) 30 min; b) and b$_1$) 120 min.

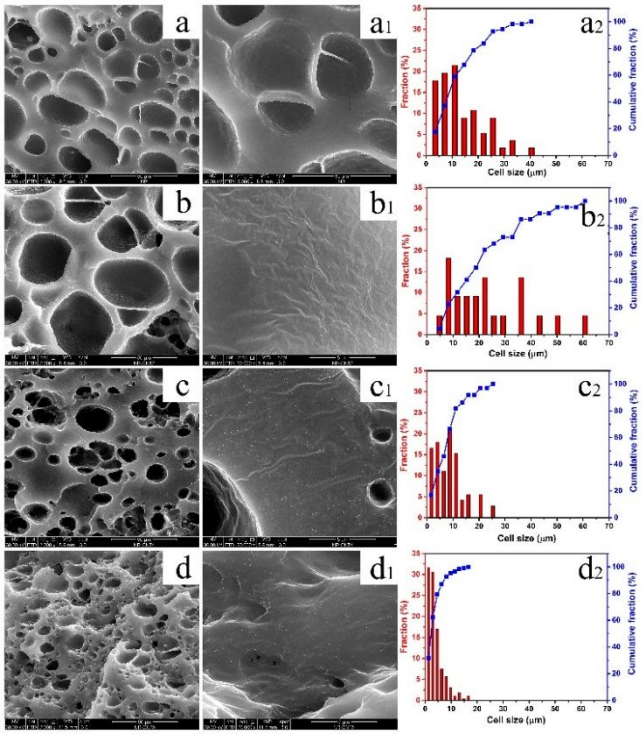

Fig. 3. Cell morphology and size distribution of F-NR/CNT composite foams with different CNT content: a), a$_1$) and a$_2$) 0 wt%; b), b$_1$) and b$_2$) 1.68 wt%; c), c$_1$) and c$_2$) 3.31 wt%; d), d$_1$) and d$_2$) 4.87 wt%. All samples are saturated at 40 bar and 35°C for 60 min. Images a$_1$), b$_1$), c$_1$) and d$_1$) are the magnified images of a), b), c) and d), respectively.

Cellular morphology of F-NR/CNTs composite foams

A series of N-NR/CNT composites with CNTs segregated network were prepared by pre-crosslinking the natural rubber particles wrapped with CNT by hot-pressing at 120 °C for 3 min. These pre-crosslinked N-NR/CNT composites were subsequently foamed by $ScCO_2$ through gas solubilization at 35 °C and expansion at room

conditions, and further crosslinked by thermal treatment at 170 °C. It is worth noting that the saturation time is a key parameter to control the cell structure of porous materials.[35] Fig. 2 and Fig. 3c) illustrate the effect of saturation time on cell morphology for the F-NR/$CNT_{3.31}$ composites. By increasing saturation time from 30 min to 60 min and then to 120 min, the mean cell diameter of F-NR/$CNT_{3.31}$ increases from 5.51 µm to 8.57 µm, and then it decreases to 6.32 µm whereas the cell density increases with the saturation time (see Table 2).

Cell morphologies of the foams with different CNTs content obtained after 60 min of gas saturation are shown in Fig. 3a)-d) whereas cell size distribution, mean cell diameter and cell density, which were calculated by using the Nano Measurer software, are shown in Fig. $3a_2$)-d_2) and Table 2. The mean cell diameter depends on the CNTs content and results to be maximum for the F-NR/$CNT_{1.68}$ composites. In particular, the mean cell diameter increases from 13.46 µm for pristine F-NR to 23.11 µm for the F-NR/$CNT_{1.68}$ composite, while the cell density decreases from 2.11×10^8 cells/cm^3 for pristine NR foam to 1.04×10^8 cells/cm^3 for F-NR/$CNT_{1.68}$ composite. This result is attributed to the strong interface force and entanglement between CNTs and rubber chains which, acting as physical crosslink point, hinder the macromolecular chains retraction of foamed rubber during the post-crosslinking treatment carried out at 170 °C. Fig. 4 shows a sketch of the mechanism involved in the stabilization of foams for the various composite foams. The pristine rubber expands to a higher extent with respect to CNTs-based composite systems. However, it is not stable and significantly loses its porous structure during the thermal crosslinking treatment mainly. The shrinkage of the structure is ascribed to the fact that the strained rubber macromolecules tend to recover their initial conformations state and the driving force is the potential increment of the entropic contribution, which significantly reduces the total free energy of the system. However, as the CNTs content increases, the composites exhibit a higher number of physical crosslinks due to π-π carbon nanotubes interactions, which contrast the gas expansion during foaming procedure and, above all, stabilize the foamed structure after cell nucleation, resulting in the formation of smaller bubbles,[31] as schematically shown in Fig. 4. Therefore, the mean cell diameter decreases from 23.11 µm to 3.92 µm when the CNT content further increases from 1.68 wt% to 4.87 wt%. Moreover, F-NR/$CNT_{4.87}$ composite show a narrower cell size distribution, as well as a higher fraction of smaller cells, with respect to F-NR/$CNT_{1.68}$ composite. This result is in agreement with the classical nucleation theory and the increment of number of smaller cells is ascribed to the increase of polymer viscosity due to the presence of a higher amount of CNTs. [17] Finally, it is worth noting that the cell walls are covered by CNTs as shown in Fig. $3b_1$), c_1) and d_1), and this confirms that the bubbles formation does not significantly affect the segregated CNTs network.

Fig. 5 shows TEM images of the CNTs segregated network of composite with 3.31 wt% of CNTs before and after foaming. In particular, Fig. 5a) confirms that the CNTs segregated network is clearly formed in the N-NR/CNTs composites prepared by latex mixing and hot pressing. The CNTs are wrapped on the surface of the rubber particles which, in turns, are homogenously distributed in the rubber matrix and form a three-dimensional conductive network. It is also worth noting that the morphology of the F-NR/$CNT_{3.31}$ composites (see Fig. 5b)) is somewhat similar to that of the composite before foaming procedure, confirming that segregated CNTs structure is not significantly affected by the bubble formation and straining of the rubber macromolecular structure. In addition, a segregated network with some defects is found in F-NR/$CNT_{1.60}$ (Fig. S3a)), while a better segregated CNT network is clearly observed in F-NR/$CNT_{6.40}$ composite (Fig. S3b)). Thus, the segregated CNTs network is somewhat stable and retains even after foaming, despite some alterations occurs as effect of the expansion process. However, the resulting network still contributes to enabling the electrical properties and EMI SE of materials (as it is shown in the following paragraph).

Density and expansion ratio of NR/CNTs composite foams

Fig. 6 shows density and expansion ratio of F-NR/CNT composite as function of CNTs content. Expansion ratio is the ratio of sample density before and after foaming [36, 37] and it depends significantly on the CNTs content and on the extent of interactions which establish between carbon nanotubes. In fact, when CNTs content is equal to 3.31 wt% and 6.40 wt%, the achieved expansion ratio is about 1.5 and 1.12, respectively. Whereas, in the case of R-NR/$CNT_{3.31}$, the expansion ratio has been found to be equal to 2.90. This confirms that the strong interface force which establish between CNTs in the segregated morphology hinders the cell growth in N-NR/CNT composites, mainly at high CNTs content. When CNT content is equal to 1.68 wt%, a higher volume expansion ratio is achieved. The high expansion ratio has negative effect on the structure of segregated network. At CNT contents lower than 1.68 wt%, the expansion ratio is lower than 2.7 because, in this condition, the shrinkage effect of the foamed structure (i.e. just after crosslinking process) prevails. This is ascribed to the lack of enough physical crosslinking which could stabilize the porous morphology against the macromolecular relaxations, whose driving force is the macromolecular conformations entropic effect (Fig. 4). These results are consistent with the morphology observed in the SEM images (Fig. 3).

Thermal and mechanical properties of F-NR/CNTs composite foams

Fig. 7a) shows DSC heating thermograms for pristine natural rubber and composite with 3.31 wt% of CNTs before and after foaming. The curves highlight that the addition of CNTs and the foaming procedure do not affect the Tg, which is comparable with that of pristine NR (around -61°C). Similar results are obtained for the other composite foams (the results are not shown for the sake of brevity). Fig. 7b) displays the thermal degradation curve of pristine natural rubber and composite with 3.31 wt% of CNTs before and after foaming. The porous structure hasn't any effect on thermal degradation mechanisms of both pristine natural rubber and composite material. However, the onset degradation temperature of F-NR/$CNT_{3.31}$ composite foam is higher than that of pristine F-NR foam and that is ascribed to the presence of CNTs which, being located around the rubber particles, contribute to thermally protect the polymer and hinder the transport of degradation gases/volatiles. [38, 39] Furthermore, during the degradation process, volatile degraded NR components may be adsorbed on CNT, leading to a delay of the mass loss, as reported for the carbon black reinforced polyester resin composites. [38] The results of thermal characterization highlight that

the CNT segregated morphology contributes to enlarge the thermal applicability window of the resulting composite foams without any detrimental effects.

Fig. 7c) shows the effect of the CNT content on the stress−strain curves until 35% of strain of F-NR/CNTs composites foams with segregated network under compression. Further information on mechanical behaviour of F-NR/CNTs composites foams at higher strains are given in Supporting Information Section (Table S1). The presence of CNTs improve significantly the mechanical properties of F-NR/CNTs composites.

The Fig. 7d shows the specific modulus, obtained dividing the corresponding measured value by the density and the hardness of F-NR/CNTs composite foams. The specific modulus of F-NR/CNTs and N-NR/CNTs composites with segregated network is shown in Fig. S4 as function of the CNT weight fraction. As already reported in literature,[40] the specific modulus of F-NR/CNTs composites is lower than that of N-NR/CNTs composites. However, the specific modulus of F-NR/CNTs increases with the CNTs content. Since the foam consists of NR or NR/CNTs composite material in the continuous phase and of gas in the dispersed phase, thus its stress-strain behaviour depends on the mechanical properties and the morphology of both phases. Therefore, the enhancement of modulus and stress result from the synergistic effect between the reinforcing effect of CNT, the cell structure (Fig. 3), and the strong filler-rubber, as well as filler-filler, interactions. The hardness of the composites foam increased from 11 to 32.5 shore A with an addition of 4.87 wt% CNT. Also, this increment in the foam's hardness can be ascribed to the effect of the CNTs which contribute with physical crosslinking to constraint NR deformability.

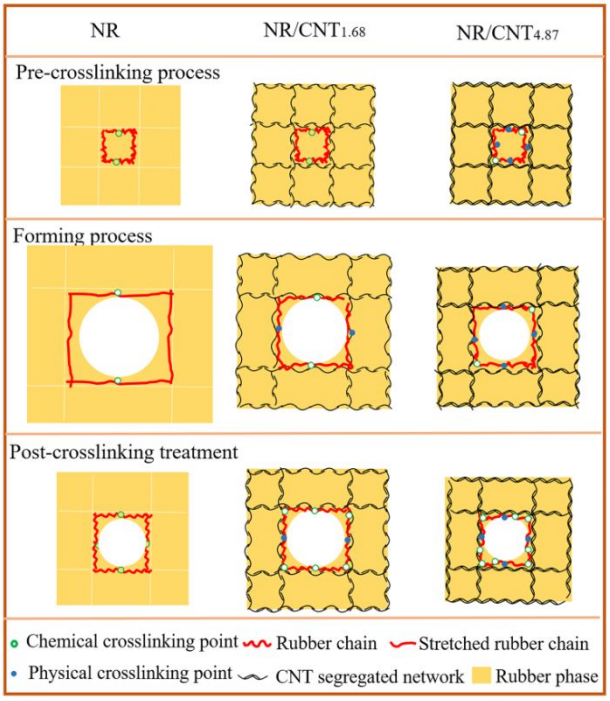

Fig. 4. Scheme of morphology for composite of NR with CNT segregated network during foaming and crosslinking process

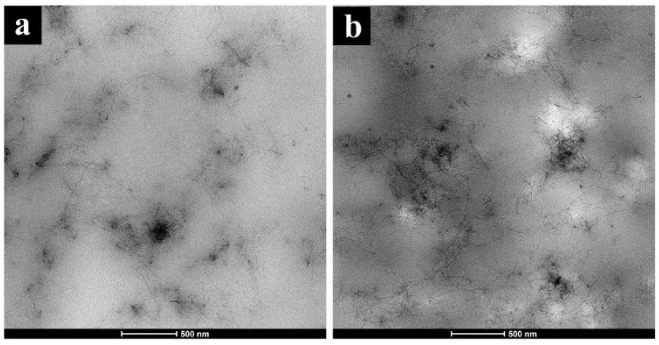

Fig. 5. TEM images of composite with 3.31 wt% of CNTs before a) and after b) foaming

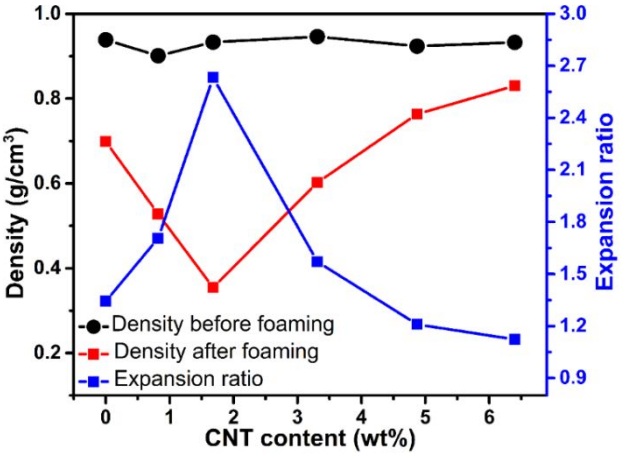

Fig. 6. Density and expansion ratio of F-NR/CNTs composite foams

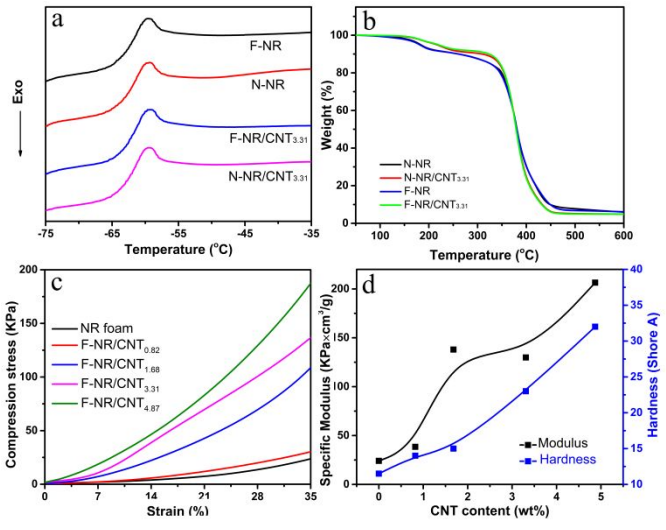

Fig. 7. a) DSC and b) TGA curves of pristine natural rubber and composite with 3.31 wt% of CNTs before and after foaming process, c) compression stress-strain curves and d) specific modulus and hardness of segregated F-NR/CNTs composite foams

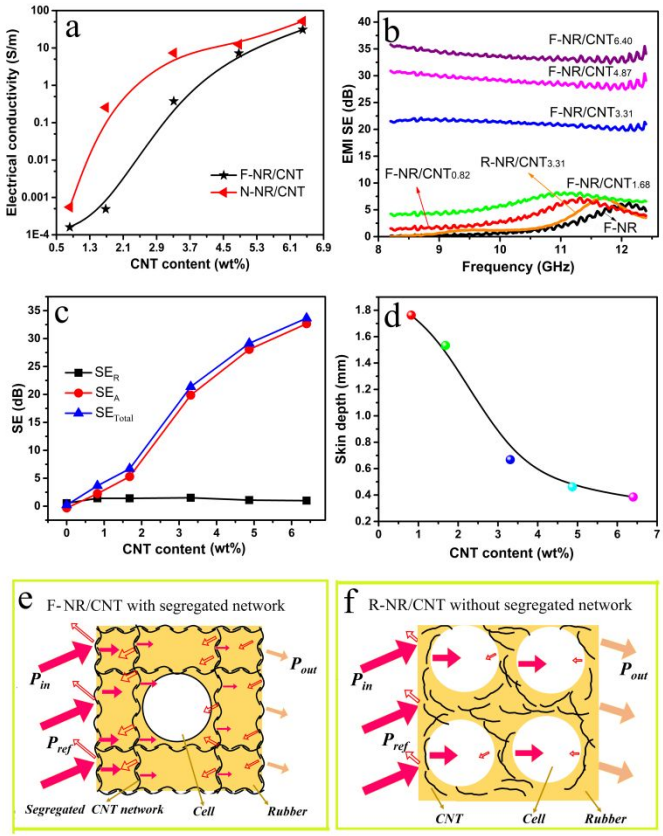

Fig. 8. a) Electrical conductivity of N-NR/CNTs and F-NR/CNTs composites with segregated network; b) EMI SE as a function of frequency for segregated F-NR/CNTs composites and R-NR/$CNT_{3.31}$ foam; c) Shielding by reflection, absorption, and total shielding of segregated F-NR/CNTs at the frequency of 10.3 GHz; d) Skin depth of materials with different CNTs content at the frequency of 10.3 GHz, e) and f) scheme of EMI shielding mechanisms for F-NR/CNTs with (ie polygonal structures) and without segregated network. $P_a=P_{in}-P_{ref}-P_{out}$, where, P_{in}, P_{ref}, P_a and P_{out} are the incoming, reflecting, absorbing and outgoing power of electromagnetic radiation, respectively.

Electrical conductivity of F-NR/CNTs composite foams

Electrical conductivity of F-NR/CNTs composite foams is one of the critical parameters which usually affect their EMI shielding performance. [8] The electrical conductivity of F-NR/CNTs and N-NR/CNTs composites with segregated network as function of the CNT weight fraction is shown in Fig. 8a). The specific electrical conductivity of F-NR/CNTs and N-NR/CNTs composites are reported, instead, in Fig. S6. As expected, the electrical conductivity significantly increases with the CNTs volume fraction. The electrical conductivity of F-NR/CNTs composites is generally lower than that of N-NR/CNTs composites. The extent of reduction depends on the expansion ratio, the higher is the expansion ratio of the composite foams the bigger is the difference in the electrical conductivity between foamed and unfoamed samples. For examples, the conductivity of F-NR/$CNT_{1.68}$ composites, which is characterized by the highest expansion ratio, is equal to 4.90×10^{-4} S/m, being significantly lower than 0.26 S/m exhibited by the N-NR/$CNT_{1.68}$ composite. This reduction may be ascribed to effect of expansion on the CNT conductive network, which becomes less effective to allow high conductivity. The electrical conductivity of F-NR/CNT with higher CNT content, however, is somewhat comparable to that of N-NR/CNT composites. Moreover, the electrical conductivity of F-NR/$CNT_{3.31}$ with segregated network is 0.38 S/m while R-NR/$CNT_{3.31}$ are not-conductive. This result is ascribed to the CNT segregated network which is preserved during $ScCO_2$ foaming procedure, as shown in Fig. 5b).

EMI shielding properties of F-NR/CNT composite foams

Fig. 8b) displays EMI SE values of segregated F-NR/CNTs in the microwave frequency range between 8.2 and 12.4 GHz. The EMI values remarkably increase with the CNTs content. The average EMI SE value for the F-NR/$CNT_{3.31}$ composites with the thickness of 1.3 mm is equal to 21.11 dB, which already satisfies the commercial EMI shielding requirement for shielding materials which is set at 20 dB. [41] Moreover, it has been found that the EMI SE of F-NR/$CNT_{6.40}$ composite reaches the excellent value of 33.74 dB, mainly due to the synergistic effect between the high electrical conductivity and the porous structure of composite foams. In fact, R-NR/$CNT_{3.31}$ shows an EMI SE somewhat comparable with that of N-NR foam. Furthermore, EMI SE of F-NR/CNTs composites with a CNT content less than 1.68 wt% shows a peculiar trend with the presence of a maximum over the investigated frequency range, which may be tentatively ascribed to both the testing environment and its porous structure. [42] On the contrary EMI values exhibit weak frequency dependence when CNTs content is higher than 3.31 wt%. The attainment of a steady SE values indicate that a homogenous and regular CNT conductive network has been formed in the composites whose structure do not depend anymore on the CNTs content. [43] Based on Table 3, SE of N-NR/CNT with low CNT content (ie., 0.82 wt% and 1.68 wt%) is almost three times higher than that of F-NR/CNT. This is attributed to the modification of the segregated network which after foaming is not effective to allow high electrical conductivity of foams. When CNT content is high, SE of F-NR/CNT foams is similar to that of N-NR/CNT composites.

It is well known that EMI SE of materials depends on the reflection and absorption of the incident electromagnetic waves. The reflection of EM wave occurs as consequence of the impedance mismatch between air and absorber material. The absorption originates from ohmic loss (i.e. attenuation of energy through the electrical current flow in phase with the applied EM wave), polarization loss (i.e. dissipation of energy by overcoming the momentum needed to reorient the dipoles in the alternated EM wave) and magnetic loss (i.e. attenuation of energy coming from magnetic particles in EM field). [2] Since rubber and CNT do not possess magnetic properties, SE_A value of F-NR/CNTs foams with segregated network depends only on the ohmic loss and polarization loss. In order to assess the EMI mechanisms of F-NR/CNTs composites with segregated network, a comparison of SE_R and SE_A is shown in Fig. 8c). The values of SE_{Total} and SE_A noticeably increase with the CNTs content, while SE_R changes only slightly over the investigated CNT content range. This confirms that absorption of electromagnetic waves plays a major role to EMI SE of F-NR/CNTs rather than reflection mechanism, [44] suggesting that most EM radiation is dissipated in form of heat. In another word, F-NR/CNTs effectively absorb and convert EM energy into thermal energy, rather than reflect them into surroundings. This result is

similar to N-NR/CNT composites (Fig. S6) as well as the findings reported for graphene/polymethylmethacrylate and CNT/epoxy composites.[45,46]

Skin depth, δ is an important parameter for the evaluation of the shielding ability of the materials. It represents the depth at which the intensity of the radiation inside the material decreases to 1/e of its original value at the surface, and it determines SE_A values of materials with a fixed thickness, d. [2, 43] The relationship between SE_A and skin depth is reported by Equation (9):

$$SE_A = 20\log(e^{d/\delta}) = 8.686(d/\delta) \quad (9)$$

The skin depth depends on the frequency according to Equation (3):

$$\delta = 1/(\pi f \mu \sigma)^{1/2} \quad (10)$$

where f is frequency, σ is electrical conductivity, and μ is magnetic permeability of materials (ie. $\mu=\mu_o\mu_r$ where $\mu_o= 4\pi \times 10^{-7}$ H/m and μ_r is material's relative magnetic permeability, $\mu_r= 1$ for the nonmagnetic NR/CNT foams). Fig. 8d) shows skin depth of F-NR/CNTs at the frequency of 10.3 GHz, which is the average value of the investigated 8.2-12.4 GHz frequency range. The skin depth sharply decreases with increasing the CNTs content. Skin depth for F-NR/$CNT_{3.31}$ and F-NR/$CNT_{6.40}$ is 0.67 and 0.38 mm, respectively. These values are much smaller than the thickness of the tested sample (1.3 mm), suggesting that the segregated F-NR/CNTs foams display an excellent EMI shielding property when CNT concentration is higher than 3.31 wt%.

In lightweight shielding applications, specific shielding effectiveness (SSE) is defined as the ratio of SE to mass density and thickness and is often used to evaluate the absolute effectiveness of shielding materials. [47] SSE of F-NR/$CNT_{3.31}$ and F-NR/$CNT_{6.40}$ composites is equal to 269.77 and 312.69 dB cm^2/g, respectively, outperforming the results of about 181 dB cm^2/g exhibited by pioneering rubber composites in the 8.2-12.4 GHz frequency band already published by some of the authors (see Table 3). Although the EMI SE of F-NR/$CNT_{6.40}$ composites is lower than that of N-NR/$CNT_{6.40}$ composites with the same CNT content (shown in Table 3), their SSE is similar with that of N-NR/$CNT_{6.40}$ composites because of the low density. In order to explain the excellent EMI shielding property of the obtained F-NR/CNTs characterized by the CNTs segregated network, a schematic description of EMI shielding mechanism is shown in Fig. 8e). On the basis of the above analysis, it is worth noting that the EMI shielding properties of segregated F-NR/CNTs depends mainly on the absorption mechanisms which originate from the ohmic loss and the polarization loss. The polarization relates to the materials' functional groups, defects, and interfaces. [2] In segregated F-NR/CNTs, the presence of rubber-gas interfaces (cells' surfaces) and CNT-rubber interfaces enhance the interfacial polarization loss which leads to the high absorption of EMI wave. The conductive three-dimensional network consequently dissipated more electromagnetic energy by ohmic losses. Thus, the F-NR/CNTs foams with segregated network behave as black hole for electromagnetic radiation which does not escape from the material before it was absorbed and transferred to heat. In other word, the excellent electrical conductivity alongside with the high numbers of interfaces, is responsible for the excellent EMI shielding property of segregated F-NR/CNTs. In addition, it has been shown in Fig. 8f) that EM wave is not absorbed by the F-NR/CNTs foams with not-segregated CNTs morphology because of the absence of the conductive network. The results display that the presence of the segregated CNT network is the crucial factor for improving EMI SE of F-NR/CNTs foams.

Conclusions

In summary, we have produced F-NR/CNTs composite foams consisting of segregated CNT network through a facile latex mixing procedure able to promote CNT wrapping around latex particles in combination with $ScCO_2$ foaming procedure. Cellular morphology and CNT segregated network, both propitious to decrease the density of composites and to improve EMI SE of materials, have been distinctly observed in the obtained foams, by SEM and TEM analysis. It has been proved that the expansion ratio of F-NR/CNTs depends on the CNT content. It exhibits a maximum value for the composite containing 1.68wt% of CNT, mainly because of physical-crosslinking between CNT and rubber. Moreover, the addition of CNT remarkably enhances electrical conductivity and EMI SE of F-NR/CNTs. More significantly, absorption efficiency plays a major role to the EMI SE of F-NR/CNTs foams rather than reflection efficiency, suggesting that most EM radiation is dissipated in the form of heat. It has been found the excellent result that SSE of F-NR/$CNT_{6.40}$ foam achieves 312.69 dB cm^2/g, outperforming the pioneering reported rubber composites in X-band frequency.

Conflicts of interest

There are no conflicts to declare.

Acknowledgements

This paper is based upon work supported by the Air Force Office of Scientific Research under award number FA9550-17-C-0116.

Notes and references

1 F. Meng, H. Wang, F. Huang, Y. Guo, Z. Wang, D. Hui and Z. Zhou, *Compos. Part B,* 2018, **137**, 260-277.
2 F. Sharif, M. Arjmand, A.A. Moud, U. Sundararaj and E.P.L. Roberts, *ACS Appl. Mater. Interfaces* 2017, **9** 14171-14179.
3 R. Sun, H. B. Zhang, J. Liu, X. Xie, R. Yang, Y. Li, S. Hong and Z. Z. Yu, *Adv. Funct. Mater.* 2017, **27**, 1702807.
4 P. Cataldi, I.S. Bayer, F. Bonaccorso, V. Pellegrini, A. Athanassiou and R. Cingolani, *Adv. Electron. Mater.,* 2015, **1**, 1500224.
5 Z. Zeng, H. Jin, M. Chen, W. Li, L. Zhou and Z. Zhang, *Adv. Funct. Mater.,* 2016, **26**, 303-310.
6 H. Zhang, G. Zhang, J. Li, X. Fan, Z. Jing, J. Li and X. Shi, *Compos. A Appl. Sci. Manuf.,* 2017, **100**, 128-138.
7 H. Pang, L. Xu, D.X. Yan and Z.M. Li, *Prog. Polym. Sci.*, 2014, **39**, 1908-1933.
8 Y. Zhan, M. Lavorgna, G. Buonocore and H. Xia, *J. Mater. Chem.*, 2012, **22**, 10464-10468.
9 Y. Zhan, Y. Meng and Y. Li , *Mater. Lett.*, 2017, **192**, 115-118.
10 N. Yan, G. Buonocore, M. Lavorgna, S. Kaciulis, S.K. Balijepalli, Y. Zhan, H. Xia and L. Ambrosio, *Compos. Sci. Technol*., 2014, **102**, 74-81.

Table 3. Specific EMI SE in 8.2-12.4 GHz frequency for the presented NR/CNT composites and the reported rubber composites

Sample	Thickness (mm)	CNT content (wt%)	SE (dB)	SSE (dB cm^2/g)	Ref.
F-NR	1.3	0	1.06	11.69	This work
F-NR/$CNT_{0.82}$	1.3	0.82	3.66	53.23	This work
F-NR/$CNT_{1.68}$	1.3	1.68	6.05	131.23	This work
F-NR/$CNT_{3.31}$	1.3	3.31	21.11	269.77	This work
F-NR/$CNT_{4.87}$	1.3	4.87	29.08	293.07	This work
F-NR/$CNT_{6.40}$	1.3	6.40	33.74	312.69	This work
N-NR/$CNT_{0.82}$	1.3	0.82	10.18	87.01	This work
N-NR/$CNT_{1.68}$	1.3	1.68	23.14	190.78	This work
N-NR/$CNT_{6.40}$	1.3	6.40	37.33	308.10	This work
CNT/NR	2.6	5.0	33.3	137.69	[12]
SBR/CNT	5	9.09	35.06	71.56	[48]
BR/CNT	1	7.41	13	14.13	[49]
NR/ENR/CB	4	23.08	23.58	63.38	[50]
TPNR/Fe_3O_4	9	12	25.52	30.48	[51]
NR/CB/silica	2.83	41.18	16.06	52.54	[52]
tire rubber/CNT	2.6	2 wt% CNT +13.1 wt% CB	36.8	152.19	[53]
NR/Fe_3O_4@GE	1.6	4.50 wt% GE +20.48 wt% Fe_3O_4	32.9	181.31	[13]

11 L.C. Jia, D.X. Yan, C.H. Cui, X. Jiang, X. Ji and Z.M. Li, *J. Mater. Chem. C,* 2015, **3**, 9369-9378.
12 L.C. Jia, D.X. Yan, Y. Yang, D. Zhou, C.H. Cui, E. Bianco, J. Lou, R. Vajtai, B. Li, P. M. Ajayan and Z. M. L, *Adv. Mater. Technol.*, 2017, **2**, 1700078
13 Y. Zhan, J. Wang, K. Zhang, Y. Li, Y. Meng, N. Yan, W. Wei, F. Peng and H. Xia, *Chem. Eng. J.*, 2018, **344**, 184-193.
14 L. Guadagno, M. Raimondo, V. Vittoria, L. Vertuccio, C. Naddeo, S. Russo, B. D. Vivo, P. Lamberti, G. Spinelli and V. Tucci, *RSC Adv.* 2014, **4**, 15474-15488.
15 B. Shen, Y. Li, D. Yi, W. Zhai, X. Wei and W. Zheng, *Carbon*, 2016, **102**, 154-160.
16 C. Liu, C. Wu, C. Hao, P. Liu, X. Guo, Y. Zhang and Y. Huang, *J. Appl. Polym. Sci.*, 2018, **135**, 45996
17 C. Forest, P. Chaumont, P. Cassagnau, B. Swoboda and P. Sonntag, *Prog. Polym. Sci.*, 2015, **41**, 122-145.
18 Y.H. Lee, C.B. Park, K. Hyun and W. Min, *J. Cell. Plast.*, 2005, **41**, 487-502.
19 D. Li and B. Han, *Macromolecules*, 2000, **33**, 4555-4560.
20 C. Zhou, N. Vaccaro, S.S. Sundarram and W. Li, *J. Cell. Plast.*, 2012, **48**, 239-255.
21 G. Gedler, M. Antunes, J.I. Velasco and R. Ozisik, *Mater. Lett.*, 2015,**160**, 41-44.
22 P. Gong, P. Buahom, M.P. Tran, M. Saniei, C.B. Park and P. Pötschke, *Carbon*, 2015, **93**, 819-829.
23 T. Mizumoto, N. Sugimura and M. Moritani, *Macromolecules*, 2000, **33**, 6757-6763.
24 G. Wang, L. Wang, L. H. Mark, V. Shaayegan, G. Wang, H. Li, G. Zhao and C. B. Park, *ACS Appl. Mater. Interfaces,* 2018, **10**, 1195-1203.
25 L. Sorrentino, E. Di Maio and S. Iannace, *J. Appl. Polym. Sci.*, 2010, **116**, 27-35.
26 H. Yan, K. Wang and Y. Zhao, *Macromol. Mater. Eng.*, 2017, **302**, 1600377
27 M. Oliviero, L. Sorrentino, L. Cafiero, B. Galzerano, A. Sorrentino and S. Iannace, *J. Appl. Polym. Sci.*, 2015, **132**, 42704.
28 Y. Zhan, J. Wu, H. Xia, N. Yan, G. Fei and G. Yuan, *Macromol. Mater. Eng.,* 2011, **296**, 590-602.
29 Y. Zhan, G. Liu, H. Xia and N. Yan, *Plast. Rubber Compos.*, 2011 **40**, 32-39.
30 A. Vahidifar, S.N. Khorasani, C.B. Park, H.E. Naguib and H.A. Khonakdar, *Ind. Eng. Chem. Res*., 2016, **55**, 2407-2416.
31 A. Vahidifar, S.N. Khorasani, C.B. Park, H.A. Khonakdar, U. Reuter, H. E. Naguib and E. Esmizadehe, *RSC Adv.* 2016, **6**, 53981-53990.
32 R. Gosselin and D. Rodriguez, *Polym Test*, 2005, **24**, 1027-1035.
33 S. Kwon, R. Ma, U. Kim, H.R. Choi and S. Baik, *Carbon*, 2014, **68**, 118-124.
34 K. Zhang, H.O. Yu, Y.D. Shi, Y.F. Chen, J.B. Zeng, J. Guo, B. Wang, Z. Guo and M. Wang, *J. Mater. Chem. C,* 2017, **5**, 2807-2817.
35 K.A. Arora, A.J. Lesser and T.J. McCarthy, *Macromolecules*, 1998, **31**, 4614-4620.
36 Y. Jia, S. Bai, C.B. Park and Q. Wang, *Ind. Eng. Chem. Res.*, 2017, **56**, 6655-6663.
37 Z. Li, Y. Jia and S. Bai, *RSC Adv.,* 2018, **8**, 2880-2886.
38 J.L. Choh, Y.C. Ching, S.N. Gan, S. Rozali and S. Julai, *Bioresource*, 2016, **11**, 913-928.

39 M.K. Alam, M.T. Islam, M.F. Mina and M.A. Gafur, *J. Appl. Polym. Sci.*, 2014, **131**, 40421.
40 J. Li, X. Liao, W. Han, W. Xiao, J. Ye, Q. Yang, G. Li, Q. Ran, *J. Supercrit. Fluid*, 2017, **130**, 198-209.
41 J.M. Thomassin, C. Jérôme, T. Pardoen, C. Bailly, I. Huynen and C. Detrembleur, *Mater. Sci. Eng. R*, 2013, **74**, 211-232.
42 Y. Xu, Y. Li, W. Hua, A. Zhang and J. Bao, *ACS Appl. Mater. Interfaces,* 2016, **8**, 24131-24142.
43 S. Mondal, S. Ganguly, M. Rahaman, A. Aldalbahi, T. K. Chaki, D. Khastgir and N. Ch. Das, *Phys. Chem. Chem. Phys.,* 2016, **18**, 24591-24599.
44 Y.J. Wan, P.L. Zhu, S.H. Yu, R. Sun, C.P. Wong and W.H. Liao, *Carbon*, 2017, **115**, 629-639.
45 H. B. Zhang, Q. Yan, W. G. Zheng, Z. He and Z. Z. Yu, *ACS Appl. Mater. Interfaces*, 2011, **3**, 918-924
46 Y. Chen, H. B. Zhang, Y. Yang, M. Wang, A. Cao and Z. Z. Yu, *Adv. Funct. Mater.*, 2016, **26**, 447-455
47 J. Ma, M. Zhan and K. Wang, *ACS Appl. Mater. Interfaces*, 2015, **7**, 563-576.
48 J. Abraham, M. Arif P, P. Xavier, S. Bose, S. C. George, N. Kalarikkal and S. Thomas, *Polymer,* 2017, **112**, 102-115.
49 N. Joseph, C. Janardhanan and M.T. Sebastian, *Compos. Sci. Technol.*, 2014, **101**, 139-144.
50 P. Zhao, L. Li, Y. Luo, Z. Lv, K. Xu, S. Li, J. Zhong, Z. Wang and Z. Peng, *Compos. Part B,* 2016, **99**, 216-223.
51 I. Kong, S.H. Ahmad, M.H. Abdullah, D. Hui, A.N. Yusoff and D. Puryanti, *J. Magn. Magn. Mater.*, 2010, **322**, 3401-3409.
52 A.A. Al-Ghamdi, O.A. Al-Hartomy, F. R. Al-Solamy, N. Dishovsky, M. Mihaylov, N. Atanasov, G. Atanasova and D. Nihtianova, *J. Polym. Res.*, 2016, **23**, 180.
53 L.C. Jia, Y.K. Li and D.X. Yan, *Carbon*, 2017, **121**, 267-273.

Specific shielding effectiveness of segregated CNT/rubber foams fabricated by supercritical CO_2 method reaches to 312.69 dB cm^2/g.